



**HAL**  
open science

## Hydrophilicity Affects Stress Response of COS-7 Fibroblast-Like Cells Exposed to Functionalised Gold Nanoclusters

Denver Linklater, Xavier Le Guével, Erim Kosyer, Sergey Rubanov, Gary Bryant, Vladimir Baulin, Eva Pereiro, Palalle G.Tharushi Perera, Jason Wandiyanto, Ana Angulo, et al.

► **To cite this version:**

Denver Linklater, Xavier Le Guével, Erim Kosyer, Sergey Rubanov, Gary Bryant, et al.. Hydrophilicity Affects Stress Response of COS-7 Fibroblast-Like Cells Exposed to Functionalised Gold Nanoclusters. *Advanced NanoBiomed Research*, 2023, 3 (4), 10.1002/anbr.202200102 . hal-04282338

**HAL Id: hal-04282338**

**<https://hal.science/hal-04282338>**

Submitted on 13 Nov 2023

**HAL** is a multi-disciplinary open access archive for the deposit and dissemination of scientific research documents, whether they are published or not. The documents may come from teaching and research institutions in France or abroad, or from public or private research centers.

L'archive ouverte pluridisciplinaire **HAL**, est destinée au dépôt et à la diffusion de documents scientifiques de niveau recherche, publiés ou non, émanant des établissements d'enseignement et de recherche français ou étrangers, des laboratoires publics ou privés.

## Hydrophilicity Affects Stress Response of COS-7 Fibroblast-Like Cells Exposed to Functionalised Gold Nanoclusters

Denver P. Linklater<sup>a,\*</sup>, Xavier Le Guével<sup>b</sup>, Erim Kosyer<sup>a</sup>, Sergey Rubanov<sup>c</sup>, Gary Bryant<sup>a</sup>, Eric Hanssen<sup>c</sup>, Vladimir A. Baulin<sup>d</sup>, Eva Pereiro<sup>e</sup>, Palalle G.Tharushi Perera<sup>a</sup>, Jason V. Wandiyanto<sup>f</sup>, Ana Angulo<sup>g</sup>, Saulius Juodkazis<sup>f</sup>, Elena P. Ivanova<sup>a,\*</sup>

<sup>a</sup>STEM College, School of Science, RMIT University, Melbourne, VIC, 3000, Australia  
Email: [elena.ivanova@rmit.edu.au](mailto:elena.ivanova@rmit.edu.au); [denver.linklater@rmit.edu.au](mailto:denver.linklater@rmit.edu.au); [s3599557@student.rmit.edu.au](mailto:s3599557@student.rmit.edu.au); [gary.bryant@rmit.edu.au](mailto:gary.bryant@rmit.edu.au); [tharushi.perera@rmit.edu.au](mailto:tharushi.perera@rmit.edu.au)

<sup>b</sup>Cancer Targets and Experimental Therapeutics, Institute for Advanced Biosciences, University of Grenoble Alpes, Grenoble, France  
Email: [xavier.le-guevel@univ-grenoble-alpes.fr](mailto:xavier.le-guevel@univ-grenoble-alpes.fr)

<sup>c</sup>Ian Holmes Imaging Centre, Bio21, University of Melbourne, Parkville, VIC Australia  
Email: [sergey@unimelb.edu.au](mailto:sergey@unimelb.edu.au); [ehanssen@unimelb.edu.au](mailto:ehanssen@unimelb.edu.au)

<sup>d</sup>Departament de Química Física i Inorgànica, Universitat Rovira i Virgili, C/ Marcel·lí Domingo s/n, Tarragona, 43007, Spain  
Email: [vladimir.baulin@urv.cat](mailto:vladimir.baulin@urv.cat)

<sup>e</sup>MISTRAL Beamline-Experiments Division, ALBA Synchrotron Light Source, Cerdanyola del Vallès, 08290 Barcelona, Spain  
Email: [epereiro@cells.es](mailto:epereiro@cells.es)

<sup>f</sup>Optical Sciences Centre, Swinburne University of Technology, Hawthorn, VIC, 3122, Australia  
Email: [jwandiyanto@swin.edu.au](mailto:jwandiyanto@swin.edu.au); [sjudkazis@swin.edu.au](mailto:sjuodkazis@swin.edu.au)

<sup>g</sup>Immunology Unit, Department of Biomedical Sciences, Faculty of Medicine and Health Sciences, University of Barcelona, Institut d'Investigacions Biomèdiques August Pi i Sunyer Barcelona, Spain  
Email: [aangulo@ub.edu](mailto:aangulo@ub.edu)

\*Corresponding author email: [elena.ivanova@rmit.edu.au](mailto:elena.ivanova@rmit.edu.au); [denver.linklater@rmit.edu.au](mailto:denver.linklater@rmit.edu.au)

Keywords: Metal nanoclusters, gold nanoclusters, nanotoxicity

## Abstract

Atomically precise ultra-small gold nanoclusters (AuNC) show great promise for biomedical application in theranostics due to their unique optical and physicochemical properties; however, the nanotoxicology concerns and potential for health risks need to be carefully considered especially considering their high diffusion and penetration in tissues and across the cellular barrier. Here, we provide new insights into the role of surface modification of 2 nm AuNC on their uptake and localisation in COS-7 fibroblast-like cells and toxicity with impact on their metabolism. AuNCs were chemically modified with either a moderately hydrophobic monodentate-thiolated molecule (AuNC-MHA) or a more hydrophilic modified-bidentate sulfobetaine zwitterionic molecule (AuNC-ZwBuEt). Growth and proliferation of COS-7 fibroblasts were assessed following exposure to either AuNC at increasing concentrations of 5, 10, 25, 50, 100 and 200  $\mu\text{g Au mL}^{-1}$ . Uptake and localization inside fibroblasts and the resultant influence on cell ultrastructure were carefully evaluated using a combination of scanning transmission electron microscopy (STEM) and cryo-soft-X-ray tomography (cryo-SXT). At concentrations of  $\geq 25 \mu\text{g Au mL}^{-1}$ , AuNC-ZwBuEt induced severe cytotoxicity in COS-7 fibroblasts. AuNC-ZwBuEt were also observed to cross the nuclear membrane; by contrast, AuNC-MHA were not cytotoxic toward fibroblast-like cells. Cryo-SXT analysis showed that fibroblasts developed an acute stress response in the form of swollen mitochondria, nuclear membrane blebbing and the formation of large cytoplasmic vacuoles as early as 1 h post-exposure. The ability of the AuNC to escape endosomes and to translocate into the nucleus and other organelles may be the cause for the observed cytotoxicity and highlights the need for further study of metal nanocluster-cell interactions.

## Introduction

Gold nanoclusters (AuNC), consisting of an assembly of a defined number of atoms (typically between tens and hundreds), exhibit distinct electronic states enabling tunable photoluminescence from ultraviolet (UV) to near-infrared (NIR/SWIR) wavelengths creating interest in AuNC for *in vitro* cell labelling and *in vivo* imaging applications[1-7]. For example, AuNC (<3 nm core diameter), protected by thiolate ligands, have recently been demonstrated to enable excellent *in vivo* computed tomography imaging, particularly of tumours[8-11]. The combination of therapy and diagnosis or imaging into a single system is known as theranostics, and as AuNCs can be tracked in real-time in various organs, this makes them an important theranostic tool[12, 13]. Their sub-nanometer size strongly impacts their interaction with biological components (i.e. protein corona[14]) and their interaction with biological barriers at the tissue and cellular levels (high diffusivity)[3, 8, 15]. Furthermore, the rapid tissue diffusion of AuNCs *in vivo* in mice is enabled by their small size and permeability, allowing accumulation in the tumour microenvironment and leading to efficient renal elimination[16]. *In vivo* experiments show that Au nanoparticles (AuNP) in the range of 5–200 nm are captured by the reticuloendothelial system (RES) for hepatic excretion [17]. By contrast, AuNC with size below the kidney filtration threshold (KFT, ca. 5.5 nm) are cleared rapidly *via* the kidneys[18]. Nevertheless, the toxicity of residual AuNC may still pose a problem when they are engineered for therapeutic and diagnostic use[19]. For instance, researchers reported a release of AuNC in blood circulation, being first sequestered in muscle tissue, indicating the importance of studying the long-term toxicity of such ultra-small particles[20].

In solution, AuNC must be electronically stabilized by a surface ligand[21]. Functionalization of the AuNC surface allows application flexibility as they can exert their action at different specific sites. However, in turn, the nano-bio interactions of AuNCs can be significantly affected by their surface chemistry, so there is a poor understanding of their structure-function relationship *in vitro*. At the cellular level, AuNC size, surface chemistry, and hydrophobicity strongly influence particle interactions with biological membranes and affect particle uptake[22-25]. For example, AuNC of 1.4 nm capped with triphenylphosphine monosulfonate (TPPMS) have been reported to provoke adverse reactions in eukaryotic cells, inducing necrosis, mitochondrial damage and oxidative stress[26]. AuNP with the same surface functionalisation but a diameter of 15 nm did not induce the same devastating response in the cell lines as ultra-small AuNCs, suggesting that the cytotoxicity of AuNCs might be size

dependent[26-28]. Similarly, smaller (13 nm) gold nanoparticles were demonstrated to be more cytotoxic toward human kidney cells than larger (60 nm) nanoparticles[29]. AuNPs, along with silver (Ag) and platinum (Pt) nanoparticles are known to cause renal toxicity[30]. Nanoparticles manifest renal toxicity through a combination of cell membrane damage, oxidative stress, mitochondrial injury, cytoskeletal changes, apoptosis and necrosis[30]; however, the differences in the mechanisms of NP cytotoxicity (dependent on particle size and surface chemistry) toward different cell types has not been addressed.

While AuNC modified for fluorescence in the NIR and SWIR regions for *in vivo* tumour imaging exhibit high renal clearance and elimination from multiple organs[10, 31], nevertheless, the fate of residual AuNC in the biological system, particularly in the kidneys, due to their role in the elimination of AuNC, at the cellular level is not clear. Indeed, the extent of fibrosis or tubulointerstitial damage within the kidneys is a key indicator of the prognosis for renal failure[32]. Thus, we aimed to study the cytotoxicity of AuNC toward African green monkey kidney-derived COS-7 fibroblast-like cells. We also aimed to clarify the effect of the AuNC functionalities on their biodistribution and cytotoxicity. In the current work, we investigated the fate of 2 nm AuNC modified with either a hydrophilic monodentate-thiolated molecule or a hydrophobic modified-bidentate sulfobetaine zwitterionic molecule to control cell membrane interactions in COS-7 fibroblasts using a combination of STEM-EDS and cryo-soft X-ray tomography.

## Material and Methods

*Synthesis of AuNCs:* Chemical products were purchased in Sigma-Aldrich (France), and deionized water was used for all synthesis. AuNC stabilized by 6- mercaptohexanoic acid (MHA,  $C_6H_{12}O_2S$ ,  $M= 148.2 \text{ g}\cdot\text{mol}^{-1}$ ) was synthesized per our previously described protocols[33]. Briefly, 500  $\mu\text{L}$  of  $\text{HAuCl}_4\cdot 3\text{H}_2\text{O}$  (20 mM) was added to 4.8 mL  $\text{H}_2\text{O}$  followed by 4 mL of the thiolated ligand MHA (5 mM). After 1 min, 500  $\mu\text{L}$  of NaOH (1M) was added dropwise. After 5 min, 200  $\mu\text{L}$   $\text{NaBH}_4$  (20 mM in 0.2 M NaOH) was introduced dropwise under mild stirring. After 4 h, purification of the AuMHA was performed using a 3 kDa cut-off filter column (Amicon). The AuNC-MHA solution was adjusted to pH 7, concentrated to 1 mg Au  $\text{mL}^{-1}$  in water and kept refrigerated until required for experiments.

A modified thioctic-zwitterion (ZwButEt,  $C_{19}H_{38}N_2O_4S_3$ ,  $M= 455.2 \text{ g}\cdot\text{mol}^{-1}$ ) was synthesized following the protocol described elsewhere[23]. Briefly,  $\text{HAuCl}_4\cdot 3\text{H}_2\text{O}$  (50 mM) was added to an alkaline solution (pH 10) containing the ligand in the presence of the reducing agent  $\text{NaBH}_4$

(50 mM) and stirred for 15 h. Zwitterion stabilized Au NCs were synthesized with the molar ratio Au: ZwBuEt: NaBH<sub>4</sub> = 1: 2: 2. Afterwards, the solution was filtered 3× with Amicon 3 kDa cut-off filters at 13,600 rpm for 20 min to remove excess free ligand, adjusted to pH 7, concentrated to 1 mg Au mL<sup>-1</sup> in water, and kept refrigerated until use.

*Mammalian cell growth conditions:* COS-7 fibroblasts were cultured in Dulbecco's Modified Eagle's medium (DMEM) (Invitrogen) supplemented with 10% fetal bovine serum (FBS) and 1% penicillin-streptomycin at 37 °C and 5 % CO<sub>2</sub>. The use of the cell line was approved by the Biosafety Project 2014/SBC01. Cells were grown to reach 80% confluency and then trypsinized using 0.25% Trypsin/ EDTA (Invitrogen) and seeded in 96-well-culture plates at 5,000 cells/cm<sup>2</sup> for each independent experiment.

*Cell Proliferation:* Cell proliferation was determined using the CellTiter 96® Aqueous One Solution Cell Proliferation Assay (Promega, Madison, WI, USA). Tetrazolium was added to the COS-7 cell culture at a 10% ratio of the final volume and incubated for 90 min at 37 °C and 5% CO<sub>2</sub>, allowing for the reduction of MTS (3-(4,5-dimethylthiazol-2-yl)-5-(3-carboxymethoxyphenyl)-2-(4-sulfophenyl)-2H-tetrazolium) to formazan, resulting in the formation of a coloured precipitate (purple). The absorbance was recorded at a wavelength of 490 nm using a FLUOstar Omega microplate reader (BMG LABTECH, Thermo Fisher Scientific, Waltham, MA, USA).

*Fluorescence Microscopy:* COS-7 fibroblast cells were incubated with AuNCs for 24 h. Afterwards, the samples were washed 3× in warm 10 mM PBS (pH of 7.4) to remove unattached AuNC and transferred to particle-free media and incubated for a further 1, 4 or 7 days. Then the samples were fixed with 4% paraformaldehyde for 15 min, permeabilised in 0.1% Triton X for 5 min, and then blocked with 1% Bovine Serum Albumin (BSA) for 60 min. Image-IT® FX Signal Enhancer (Invitrogen, Carlsbad, CA, USA) was also used during the fixation stage to enhance the subsequent fluorescent signals. Actin filaments were visualised by staining the cells with Alexa Fluor 488 conjugated phalloidin (Invitrogen). Cell nuclei were labelled using TO-PRO3 (Invitrogen). Samples were then imaged using a Fluoview FV3000 microscope (Olympus, Tokyo, Japan) at 60× magnification.

*Transmission Electron Microscopy (TEM):* TEM was used to view cross-sections of COS-7 fibroblasts incubated with AuNCs. COS-7 fibroblasts were exposed to 100 µg/ml AuNCs for

24 h. Following the incubation period, the cells were washed to remove non-adherent particles in PBS and then incubated in particle-free media for a further 1-, 4-, or 7-days post AuNC exposure. The cells were then fixed for TEM preparation as previously described [34]. Briefly, after incubation, cell suspensions were washed to remove any nanoparticles that had not interacted with the cells. The pellets were then fixed using 4% paraformaldehyde in PBS for 15 min and then washed twice in PBS. The cells were post-fixed with 1% aqueous osmium tetroxide ( $\text{OsO}_4$ ) for 1.5 h. Samples were then washed and dehydrated by passing them through a graded ethanol series (20, 40, and 60%) (2 mL) for 20 min each concentration. The cells were retained overnight in 2% uranyl acetate in 70% ethanol. After staining, the cells were fully dehydrated using ethanol at concentrations of 80, 90 and 100% for 15 min each. The embedding medium was prepared using Spurr's resin (ProSciTech) and embedded according to the manufacturers protocol. Each sample was polymerized for 24 h at 4°C. The final block was trimmed and then cut into ultrathin sections (50 nm thickness) using a Leica EM UC7 Ultramicrotome (Leica Microsystems, Wetzlar, Germany) with a diamond knife (Diatome, Pennsylvania, USA). Sections were placed onto 300 mesh copper grids and examined using a JEM 1010 instrument (JEOL).

STEM-EDS analysis was performed on samples prepared as described above using a TEM Jeol 2100F (FEG, 200 kV) equipped with a high-angle annular dark field detector (HAADF, scanning TEM mode, STEM) and energy dispersive X-ray spectrometer (EDS).

*Cryo-soft-X-ray tomography:* Prior to cell seeding, hydrophilization of quantifoil R 2/2 holey carbon-film Au microscopy grids (Au-G200F1) was achieved by exposure to 1 min  $\text{O}_2$  plasma.  $2 \times 10^4$  COS-7 fibroblasts were seeded onto each grid in a 96-well-plate (Corning) and incubated for 24 h prior to exposure to AuNC. After 1 h of exposure to  $100 \mu\text{g Au mL}^{-1}$  AuNC, Au grids with adhered cells were washed gently with warm PBS and stained for 5 min with Mitotracker (Thermofisher Scientific).

Immediately before plunge-freezing (Leica, EM, GP), 2  $\mu\text{L}$  of 100 nm diameter Au fiducial markers were added to the grids for tomogram alignment. The grids were then blotted from the rear using Whatman filter paper no.4 to remove the excess medium. The cell distribution and the ice thickness were examined using a cryostage (CMS196 Linkam Scientific Instruments, Epsom, UK)-equipped fluorescence microscope (Zeiss Axio Scope). Grids were transferred to cryo-boxes and stored in liquid nitrogen.

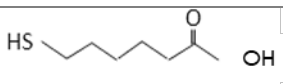
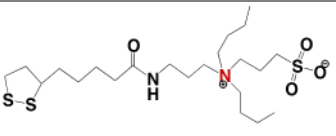
The grids were imaged using the Mistral (ALBA-Light Source) beamline at the ALBA synchrotron (Barcelona, Spain) under cryogenic conditions. Tomography was performed over a tilt range of  $\pm 65^\circ$  with a step size of  $1^\circ$  at 2.43 nm wavelength (photon energy  $E = 520$  eV). Image collection was performed using a 25 nm zone and a 25 nm plate, and an image pixel size of 10 nm. Approximately  $\sim 131$  images were acquired for each tilt series with exposure times varying from 1s-2s. Tilt series were aligned, reconstructed and segmented using IMOD software.

*Statistical analysis:* Data are expressed as the mean  $\pm$  one standard deviation (SD) of at least 5 independent replicates (n). Statistical comparisons were made between results using a two-tailed Student's T-test where  $p < 0.05$  denoted a statistically significant difference.

## Results

AuNCs of 2 nm diameter were synthesised according to a previously optimised protocol[33] and functionalized with a moderately hydrophobic monodentate-thiolated molecule, mercaptohexanoic acid (MHA) containing a short aliphatic chain with a terminal carboxyl group)[35-37] and a more hydrophilic modified-bidentate sulfobetaine zwitterionic molecule (ZwBuEt)[23]. Their respective surface characteristics are shown in Table 1. AuNC-MHA and AuNC-ZwBuEt have demonstrated good colloidal stability in water, buffer solution and serum-containing medium for great lengths of time ( $\sim 6$  months)[12, 23, 38, 39].

**Table 1. Surface characterisation of AuNC**

AuNC	Ligand Structure	Size* <sup>[34]</sup>	Zeta Potential ( $\zeta$ )** <sup>[23]</sup>	Surface ligand logP
MHA		Width = 0.73 nm, length = 2.27 nm	-21.3 $\pm$ 0.5 mV	1.43
ZwBuEt		Width = 0.79 nm, length = 2.32 nm	-10.0 $\pm$ 0.2 mV	-3.45

\*as determined by SAXS measurements and includes Au core + ligand

\*\* at pH 7 in H<sub>2</sub>O



### **AuNC cytotoxicity toward COS-7 fibroblasts**

To assess the corresponding cytotoxicity of AuNC in COS-7 fibroblastic cells, we performed cell proliferation (MTS) assays following acute exposure (after 24 h) and 4- and 7-days post-exposure to AuNCs functionalised with either MHA or ZwBuEt ligands to investigate cell recovery (or chronic impact) (Figure 1A)[40]. Cell viability and metabolic activity were assessed compared to the untreated (no AuNC exposure) sample by reducing the tetrazolium salt compound by viable cells to a coloured formazan dye. The colour change is relative to the number of living cells and corresponds to the metabolic activity of the cells. At 24 h after exposure, at 25  $\mu\text{g mL}^{-1}$ , AuNC-MHA showed no detrimental effect on cell viability as determined by no decline in the percentage of cell metabolic activity compared to the non-treated cells. However, at higher concentrations ( $>50 \mu\text{g mL}^{-1}$ ), AuNC-MHA influenced COS-7 fibroblast metabolism after a 1-day exposure. There was a 30% reduction in cell metabolic activity at concentrations of 50 and 100  $\mu\text{g mL}^{-1}$  ( $p \leq 0.0004$  and  $p \leq 0.0008$ , respectively). Those cells exposed to 200  $\mu\text{g mL}^{-1}$  experienced increased cell metabolic activity; however, this was not corroborated at day 4- post-exposure and cells exhibited decreased proliferation (approximate reduction of 30 % in comparison to the control ( $p < 0.005$ ). Nevertheless, by day 7, COS-7 fibroblasts had recovered from AuNC-MHA exposure, and there were no statistically significant differences in cell metabolic activity between treated and non-treated samples. Increased cell metabolic activity upon nanoparticle exposure has been associated with abnormal mitochondrial function [41].

By contrast to AuNC-MHA, AuNC-ZwBuEt at the maximum concentration of 200  $\mu\text{g Au mL}^{-1}$  induced a statistically significant reduction in cell metabolic activity of  $\sim 50\%$  ( $p < 0.0005$ ) after 24 h of exposure, whereas lower concentrations failed to impact cell metabolism negatively. However, by day 4, those cells treated with  $\geq 100 \mu\text{g Au mL}^{-1}$  showed substantial reductions in cell proliferative activity. In addition, cell proliferation of those fibroblasts incubated with  $\geq 100 \mu\text{g Au mL}^{-1}$  AuNC-ZwBuEt was reduced by 60%. By day 7, there was an improvement in cell culture conditions; however, cell metabolism remained below that of the untreated sample (although the difference was not statistically significant), indicating the reduced metabolism of MTS by COS-7 fibroblasts exposed to AuNC-ZwBuEt was a result of AuNC toxicity.

Actin staining was used to reveal the morphological changes to the cell cytoskeleton induced by AuNC exposure at concentrations of  $\geq 100 \mu\text{g Au mL}^{-1}$  for 24 h and following recovery for

4 days. Fluorescence micrographs confirm that 24 h exposure to concentrations of  $100 \mu\text{g Au mL}^{-1}$  AuNC-MHA does not adversely affect the cytoskeletal network of COS-7 fibroblasts. CLSM micrographs show normal cellular morphology and cell spreading (Figure 1B, C). However, those cells exposed to AuNC-ZwBuEt exhibit a highly rounded morphology at day 1 with a disorganised actin network and more radial actin fibres than polarised actin fibres (Figure 1B, Figure 1C). Previously the uptake of 40 nm AuNPs has been associated with the cytoskeletal remodelling of endothelial cells[42]. By day 4, those cells treated with AuNC-MHA exhibited normal cell spreading and migration, indicating recovery from AuNC exposure (Figure S1). Nevertheless, at day 4, AuNC-ZwBuEt treated cells' proliferation rate is stunted, as the MTS assay and cell number have not increased substantially from day 1 to day 4. Indeed, at higher concentrations ( $200 \mu\text{g Au mL}^{-1}$ ), CLSM micrographs show that COS-7 cells fail to form cell surface extensions filopodia compared to untreated cells (Figure S2). It has been hypothesised that cell apoptosis following AuNCs exposure results from the number of vacuoles in the cells, which may disrupt the cytoskeleton, causing cell area contraction and decreased motility[43].

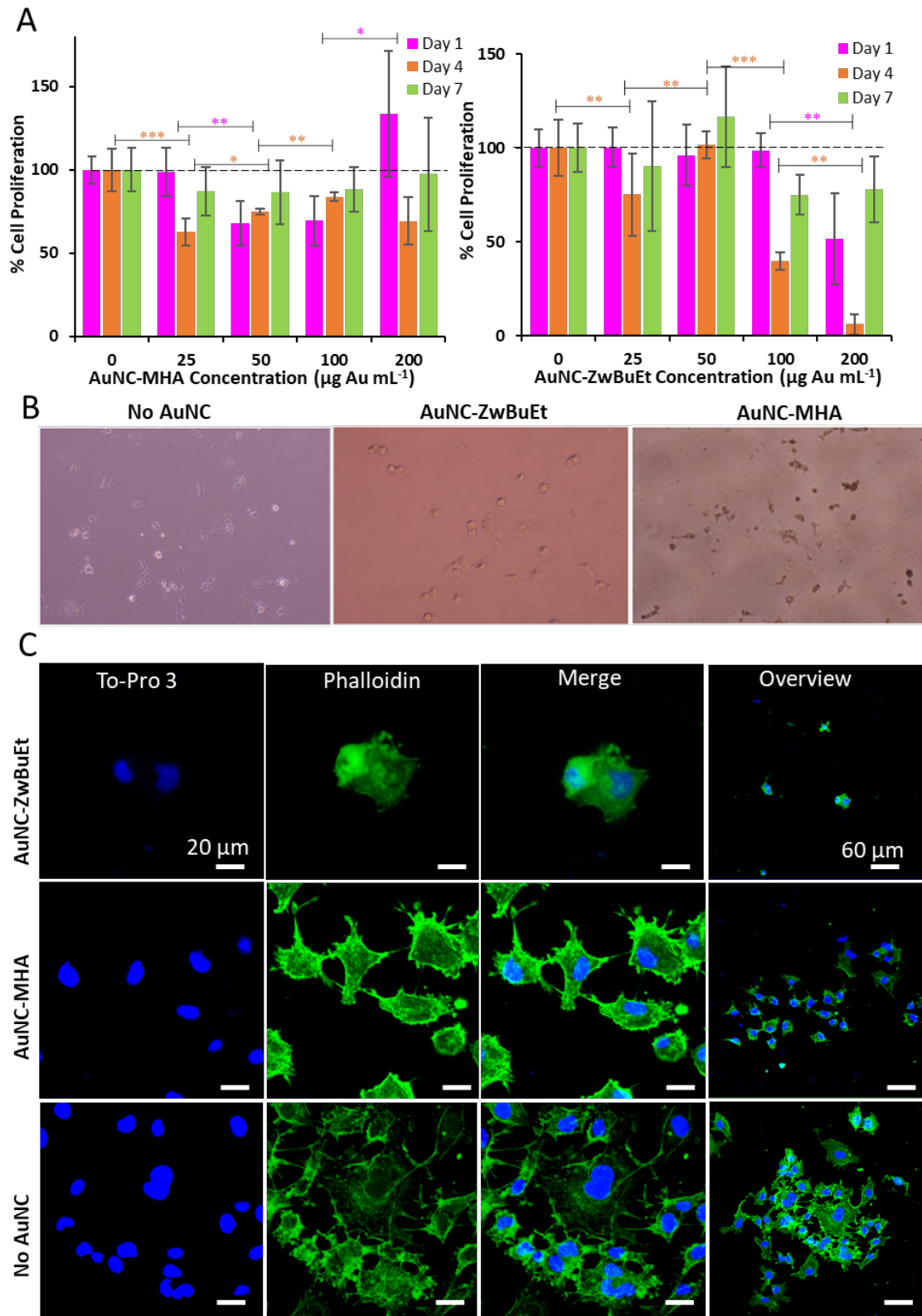


**Figure 1.** Viability of COS-7 fibroblasts incubated with AuNCs for 24 h and 4- and 7-days post-exposure. (A) Evaluation of the cell metabolic activity in the presence of AuNC-MHA and AuNC-ZwBuEt at concentrations of 25, 50, 100, to 200  $\mu\text{g Au mL}^{-1}$  by MTS assay as a percentage of the control. Results are presented as the mean  $\pm$  standard error ( $n = 3$ ) ( $***p <$

0.005,  $**p < 0.01$  and  $*p < 0.05$ ). (B) Optical micrographs of COS-7 fibroblasts in culture post 24 h exposure to  $100 \mu\text{g Au mL}^{-1}$  AuNCs. The colour difference between the respective photographs can be attributed to adding AuNCs to cell media. COS-7 fibroblasts incubated with AuNC-MHA appear to be coated with particles. (C) CLSM micrographs of the morphology of COS-7 fibroblasts 24 h exposure to  $100 \mu\text{g Au mL}^{-1}$  AuNCs. The nucleus is stained with To-Pro 3 (blue); the actin network is stained with Phalloidin (green).

### **Surface-ligand-dependent uptake of AuNC**

TEM and STEM-EDS analysis of COS-7 fibroblasts exposed to AuNCs was used to confirm the presence of AuNC in cells and to identify changes to the cell ultrastructure (Figure 2). The TEM analyses clearly show that for AuNC-ZwBuEt, the particles are mostly sequestered inside large vesicles (lysosomal vacuoles (LV) [44]) at both days 1 and 4 post-exposure (Figure 2B) and rarely found free within the cytoplasm. No AuNC-MHA were observable within the cells at any studied time points. In AuNC-ZwBuEt-treated cells, the vacuoles are distributed uniformly across the cytoplasm. We measured the size of the vesicles containing AuNCs and AuNC aggregates, as well as the size and density of the clusters within each LV. Aggregates of AuNC-ZwBuEt have a broad size distribution of 10 – 500 nm (with an average of  $185 \pm 132$  nm) on day 1; this distribution was reduced by day 4 with AuNC-ZwBuEt aggregates possessing an average diameter of  $287 \pm 107$  nm. There was no difference in the size of the vesicles on day 1 and day 4 (Figure 2C). The larger AuNC aggregate sizes, in combination with the similarity in size of the LV, indicate that there is an accumulation of AuNC within the vesicles and that cells cannot efficiently transport the AuNCs out of the cell, even after 4 days post-AuNC exposure. STEM EDS confirmed that the contents of the LVs were mainly free AuNC and aggregates of AuNC (Figure 2A).

Similarly, there was no difference in the diameter of free AuNC that we were able to be detected by microscopy within the cytoplasm. The morphology of untreated COS-7 fibroblasts is shown in Supplementary Figure S3. Close examination of STEM images also revealed that after 4 days, particles were detected inside the nucleus (Figure 3A), as confirmed by STEM-EDS. By contrast, AuNC-MHA was not detected inside the cells through TEM or STEM-EDS analysis. In addition, cell vacuolisation and numerous endocytic vesicles were not identified within the cell cytoplasm for those cells exposed to AuNC-MHA, as was observed for those exposed to AuNC-ZwBuEt.

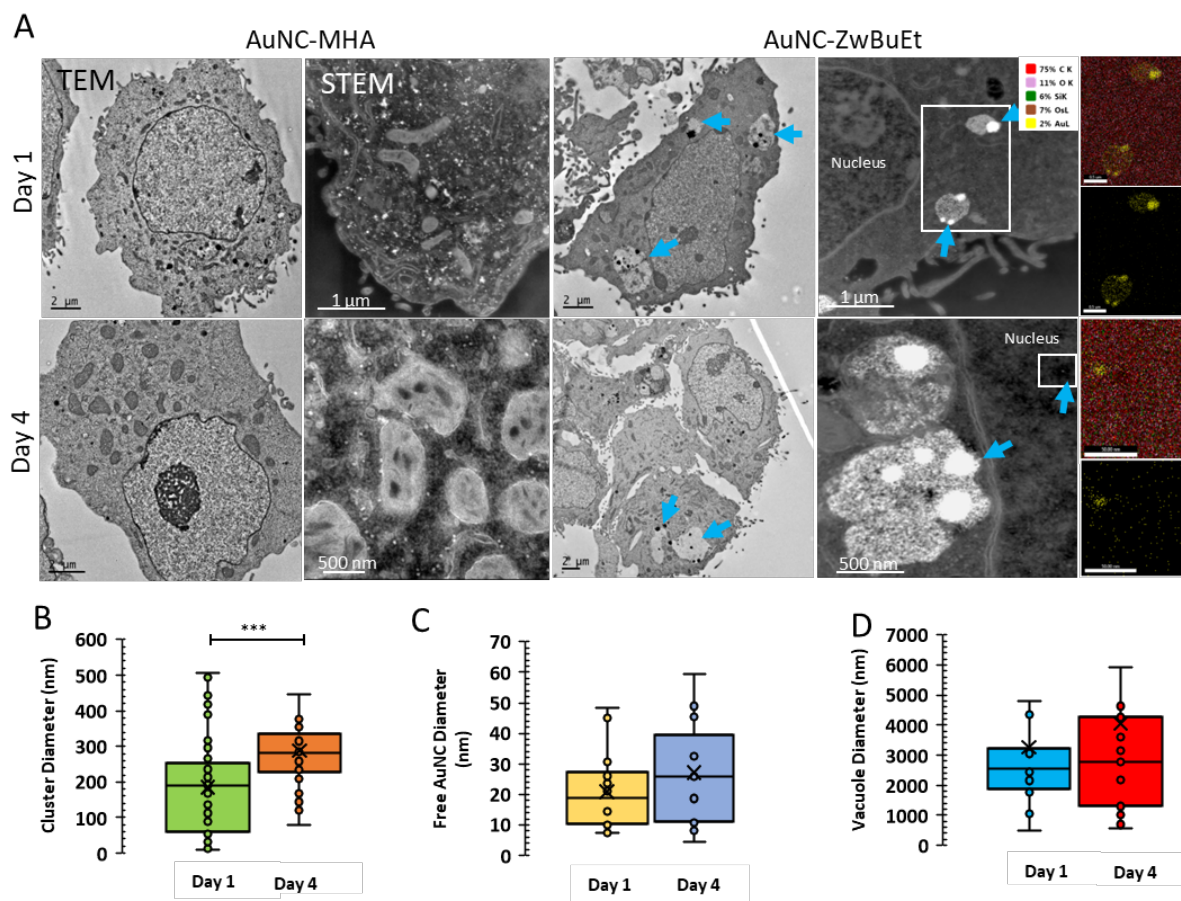


**Figure 2.** (A) TEM and STEM micrographs of COS-7 fibroblasts 1- and 4-days post-exposure to  $100 \mu\text{g Au mL}^{-1}$ . Blue arrows indicate the presence of clusters of AuNCs in vesicles and within the cell nucleus. The presence of AuNC was confirmed by STEM/EDS elemental maps (right panels). Quantification of (B) AuNC-ZwBuEt aggregate diameter localised inside vesicles, (C) AuNC-ZwBuEt diameter localised within the cell cytoplasm and (D) vacuole diameter. Data were determined from examination of 50 images. Vacuoles were measured on the long axis. Statistical significance is denoted by \*\*\*  $p < 0.0005$ ,  $n = 50$ . At 1- and 4-days post AuNC exposure, no AuNC-MHA were found localised within the cell cytoplasm or sequestered in vesicles.

### Cryo-SXT investigation of the morphology of COS-7 fibroblast ultrastructure following AuNC uptake

Cryo-SXT experiments to assess the resultant morphology and changes in ultrastructure to COS-7 fibroblasts were conducted with COS-7 fibroblast cells grown adherently on formvar-coated gold grids exposed to  $100 \mu\text{g Au mL}^{-1}$  AuNC for 1 h (Figure 3). The 1 h incubation point was used to capture the initial interactions between the AuNC and cells and to pinpoint initial changes in cell ultrastructure in response to AuNC uptake compared to control COS-7

fibroblasts (Figure S5). Figure 3B displays selected slices of tomographic reconstructions together with the segmented volume of the fibroblast, highlighting the localisation of AuNC in representative fibroblast cells. The reconstruction and segmentation of tomograms permitted analysis of the amount and location of internalized AuNC. After exposure to AuNC-MHA for 1 h, COS-7 fibroblast cell ultrastructure appears morphologically normal, although there is an increase in the number of endosomes present within the cytosol (of size  $990 \pm 186$  nm)[45]. Multiple endosomes are present in the cell cytoplasm that all possess AuNC aggregates with an average size of  $31.5 \pm 5.0$  nm.

Furthermore, autophagic vesicles were identified as ones containing membrane-bound vesicles[46]. This result contrasts with the TEM and STEM analyses above that identified no AuNC-MHA localised within the cell cytoplasm or sequestered in vesicles. At 1 h, AuNC-MHA is confined chiefly to different intracellular compartments, such as endosomes and autophagosomes, limiting their interaction with ribosomes and mitochondria in the cytosol[47]. These compartments are crucial for eliminating NPs via extracellular vesicles from the cell cytoplasm[47], suggesting that AuNC-MHA are efficiently transported out of the cell without causing significant deleterious effects.

By contrast, after exposure to  $100 \mu\text{g Au mL}^{-1}$  AuNC-ZwBuEt for 1 h, COS-7 fibroblasts showed an extreme stress response. Large numbers of vacuoles can be observed in the cytoplasm, and the mitochondria appear severely swollen and enlarged (Figure 4A, C). Mitochondrial morphology is directly related to cellular health. Segmentation allowed for the evaluation of the volume and shape of these organelles to obtain statistical information about morphological changes to the mitochondria after exposure to either AuNC-ZwBuEt or AuNC-MHA. The mitochondrial volume of AuNC-ZwBuEt treated cells in Figure 4D demonstrates a significant increase in the size of mitochondria ( $p < 0.01$ ). Previous research has shown that AuNCs exert detectable adverse effects on mitochondria. For example, human astrocytes treated with  $10 \mu\text{M}$  glutathione functionalised AuNC (AuNC-SG) of different core sizes increased the number of *elongated* mitochondria suggesting a re-balancing of mitochondrial fusion and fission[48]. In another example, cationic 5 nm AuNPs induced the formation of large vacuoles in the cytoplasm and caused the mitochondria to swell due to defective mitochondrial fission[49]. These observations are corroborated in the current work, where swollen mitochondria are indicative of cellular stress (particularly oxidative stress[50]) and mitochondrial dysfunction[45, 48, 51]. Cell vacuolisation after NP treatment has been linked to the cell opening transmembrane water channels that allow an influx of external water[52].

Additionally, autophagic compartments, or multi-vesicle bodies (MVBs), containing AuNC aggregates are observed in large numbers (Figure 4B), indicating the trigger of cell autophagy[53]. The nuclear membrane also shows signs of blebbing, which may be related to the beginning of cell apoptosis [54] (Figure 3, Figure 4). AuNC-ZwBuEt aggregates were also free within the cytoplasm (Figure 4B), either due to passive translocation across the cell membrane or endosomal escape[55].

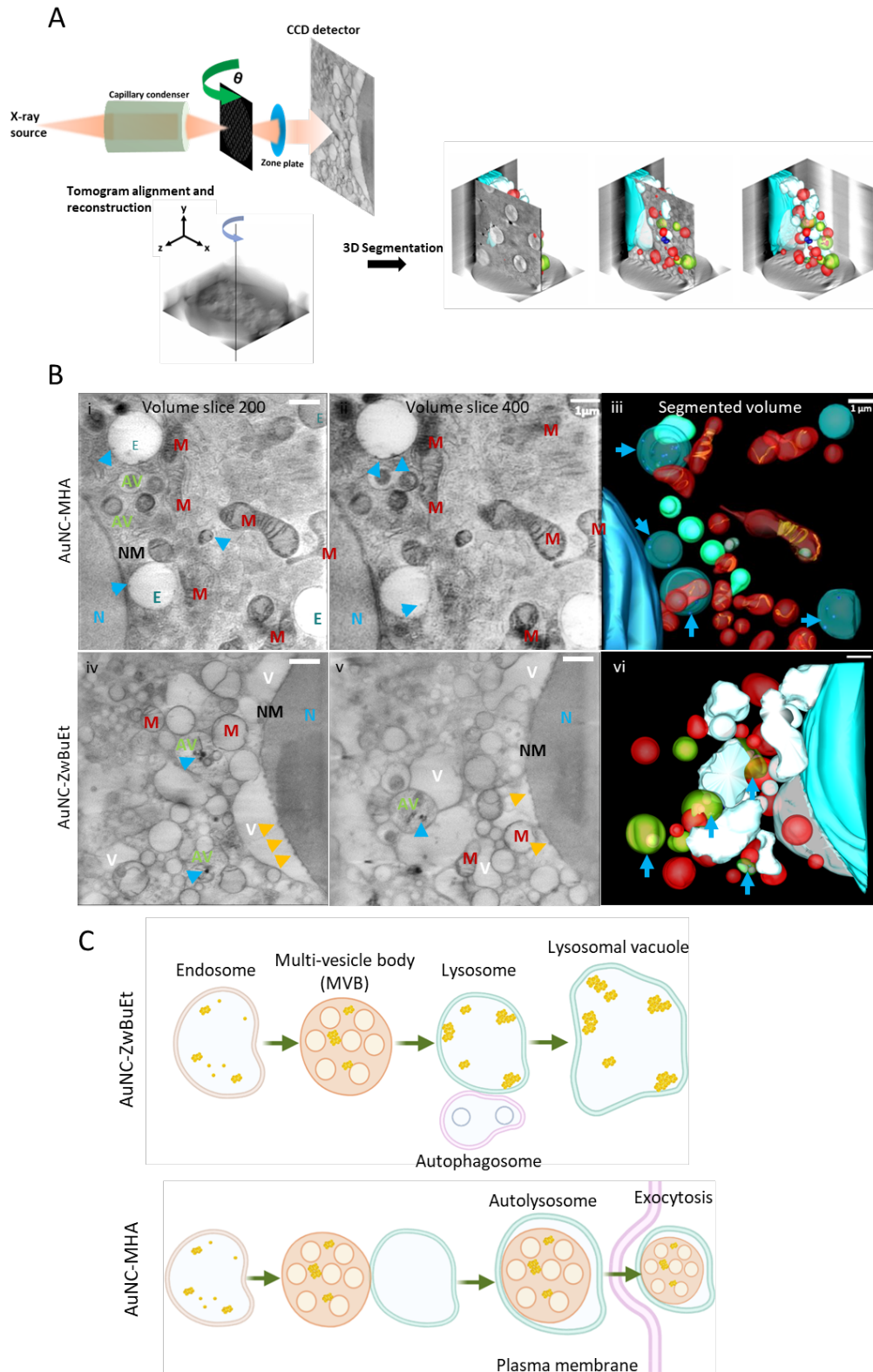


**Figure 3.** (A) Schematic representation of the cryo-SXT set-up at the Mistral beamline, ALBA. (B) Selected slices of aligned cryo-SXT tomograms and segmentation highlighting the effect of AuNCs on COS-7 fibroblast ultrastructure. Cells were exposed to  $100 \mu\text{g Au mL}^{-1}$  for 1 h prior to vitrification. Cyan arrows indicate the presence of AuNCs (in aggregates), and orange



arrows indicate examples of cell damage. Those cells exposed to AuNC-ZwBuEt experienced significant changes to cell ultrastructure, including a higher number of intracellular vacuoles and blebbing of the nuclear membrane (orange arrows). M – mitochondria, E – endosome, AV – autophagic vesicle, L- liposome, NM – nuclear membrane, N – nucleus, V - vacuole. (C) schematic of the proposed aggregation pathway of AuNC-ZwBuEt *versus* AuNC-MHA in COS-7 fibroblasts. Zwitterionic AuNCs form clusters in endosomes and multi-vesicle bodies before coalescing into larger aggregates in lysosomes. Autophagosomes merge with lysosomes to form autolysosomes. Lysosomal dysfunction leads to the formation of lysosomal vacuoles [44]. By contrast, AuNC-MHA is colocalised to autolysosomes and is exocytosed.

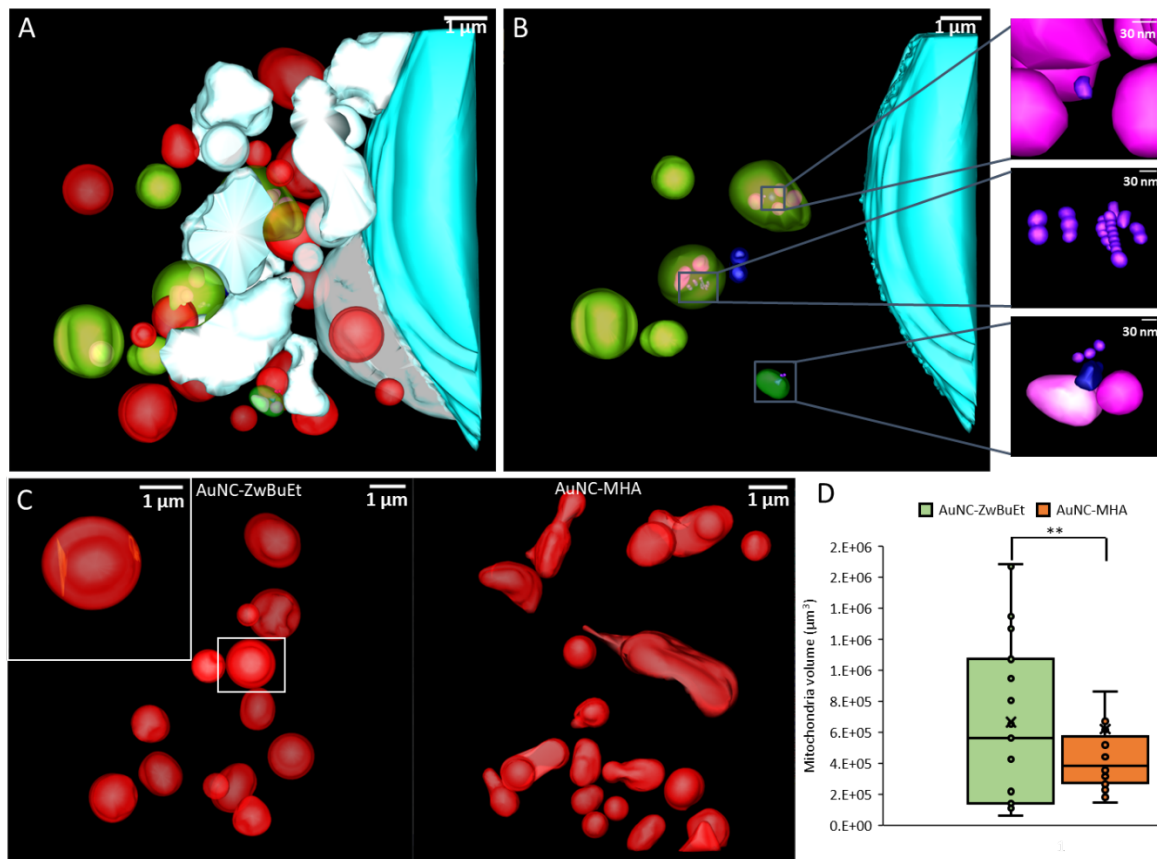


**Figure 4.** Segmentation of cryo-SXT tomogram of COS-7 fibroblasts exposed to 100 µg Au ml<sup>-1</sup> AuNC-ZwBuEt for 1 h. (A) Colour segmentation of organelles of COS-7 fibroblast. (B) Colour segmentation showing autophagic vesicles and nucleus of COS-7 fibroblast exposed to 100 µg Au ml<sup>-1</sup> AuNC-ZwBuEt. Inset images show the localisation AuNC-ZwBuEt clusters. (C) Comparison of mitochondrial morphology of fibroblasts following exposure to AuNC-ZwBuEt or AuNC-MHA. (D) Graph comparing the volume distribution of mitochondria in

COS-7 fibroblasts following AuNC exposure. Statistical significance is denoted by  $**p < 0.01$ ,  $n = 20$ .

## **Discussion**

The current study demonstrated the importance of surface chemistry for the cytotoxicity of AuNCs toward fibroblastic cells. While moderately hydrophobic MHA-modified AuNCs were relatively non-cytotoxic toward COS-7 fibroblasts, hydrophilic zwitterionic AuNC elicited pronounced cytotoxicity in fibroblasts. Indeed, the interactions at the cell-AuNC interface seem to be highly influenced by the type of ligand coating the particles. The cellular uptake of nanoparticles is the first step toward inducing a cytotoxic response in mammalian cells and is influenced by initial nanoparticle-membrane interactions, which are further governed by surface chemistry [56, 57]. Our results showed that the AuNC-MHA triggered autophagy, evidenced by Cryo-SXT revealing the presence of autophagic vesicles in the cell cytoplasm at 1 h post AuNC exposure. However, although endocytosis was not explicitly shown, AuNC-MHA were not evident within the cell cytoplasm or colocalised in endo/lysosomes at 24 h or 4 days post AuNC exposure. By contrast, the autophagic cytoprotective response triggered in those fibroblasts exposed to AuNC-ZwBuEt was overwhelmed by an apoptotic response, ultimately leading to the cell's demise. At higher concentrations ( $\leq 100 \mu\text{g mL}^{-1}$  AuNC-ZwBuEt), cell apoptotic response was evidenced by the formation of large intracellular vacuoles, nuclear blebbing and mitochondrial swelling. Cell necrosis in fibroblasts exposed to AuNC-ZwBuEt was only triggered at higher concentrations of AuNC. Indeed, cell viability assays performed at 24 h, 4 and 7- days post-exposure show that at  $\geq 100 \mu\text{g mL}^{-1}$  metabolic activity of the cells is initially reduced compared to non-treated cells, and the cells fail to recover normal proliferative behaviour at 4 days post-treatment. The cytoskeletal organisation was also impacted as F-actin staining revealed substantial changes to cell shape. Fibroblasts were highly rounded, with radial actin fibres, as opposed to possessing a highly polarised morphology[42].

As determined in this study, surface chemistry is a crucial factor influencing the biological effect of AuNCs. Firstly, protein coating of the AuNC surface in culture may influence their interactions with the cell membrane and their ultimate uptake and fate within the cell. Nevertheless, it was recently shown that coating the AuNC surface with the ZwBuEt molecule resulted in increased colloidal stability in biological medium with high protein content and an efficient translocation of the coated particle through phospholipid

membranes[23]. Indeed, coating particles with zwitterionic or PEGylated molecules has been shown to strongly reduce the formation of a protein corona and increase their half-life in blood[58]. This leads to a significant improvement in their cellular uptake [10]. Furthermore, as AuNC-ZwBuEt were detected both free within the cytoplasm and the nucleus, energy-independent free translocation and endocytic processes may occur.

The NC surface-ligand density is assumed to be different using a monothiol linker such as MHA as opposed to the bidentate thiol linker used for ZwBuEt. We previously determined the size and the composition of AuNC-MHA and AuNC-ZwBuEt by electrospray mass spectrometry with a molecular weight of 7.5kDa[59] and 13kDa[60], respectively. We also performed SAXS measurements achieving shape parameters for AuNC-MHA of a square prism with 0.73 nm sides and a length of 2.27 nm and for AuNC-ZwBuEt, a square prism with sides of 0.79 nm and a length of 2.32 nm[61]. A modified Brust-Schiffrin method was used to synthesize the particle with an excess of ligand to ensure the complete covering of the ligand on the AuNC surface, resulting in a negative surface charge (-21mV for AuNC-MHA and -10mV for AuNC-ZwBuEt, Table 1) for both NCs and high colloidal stability. Prior research has shown that thioctic molecules used as a linker led to an approximately 4-fold decrease of ligand density compared to short monothiol molecules like mercaptopropionic acid (1.72 compared to 6.26 ligand per nm<sup>2</sup> for gold nanoparticle with 12 nm diameter[62]). We found a similar trend by XPS measurements between AuNC-MHA and AuNC-ZwBuEt [59, 60] with ~ 4 times less sulphur involved in the binding of ZwBuEt to the gold surface compared to MHA. Thus, it could be that the particles synthesized with MHA ligands have fewer free gold surface atoms, thereby lowering the surface activity in comparison to AuNC-ZwBuEt. However, it is not prudent to only consider the first anchoring to the gold surface as the terminal group of the ligands completely covers the metal core, which will be in contact with the cell surface.

While Au nanoparticles of size 2-8 nm are known to passively interact with lipid membranes regardless of their surface charge[63-65], recently, we demonstrated the surface-ligand-dependent uptake of AuNC-MHA and AuNC-ZwBuEt and their consequent bactericidal activity to be related to AuNC hydrophobicity and lipophilicity. The antibacterial action of AuNC-MHA (with greater surface hydrophobicity/lipophilicity) toward *Pseudomonas aeruginosa* and *Staphylococcus aureus* bacterial cells was linked to their ability to translocate across the bacterial membrane freely and to bind to subcellular structures such as the bacterial

cytoskeleton (and other proteins)[33]. On the other hand, AuNC-ZwBuEt were observed to form aggregates at the membrane before being localised within the cell cytoplasm. Using a model membrane (DOPC lipid bilayer produced in a microfluidic device), the authors previously showed that hydrophilic AuNC-ZwBuEt could freely enter the bilayer [66]. Herein, uptake of AuNC-ZwBuEt and AuNC-MHA was assumed to be *via* endocytosis, although AuNC-ZwBuEt may be able to passively cross lipid bilayers, as evidenced by their localisation within the nucleus. Previously, the authors showed that the uptake kinetics of AuNCs protected by ligands of increasing hydrophobicity in human primary glioblastoma and melanoma cell lines highly depended on the ligand and cell line type. Cell uptake was greatest for zwitterionic AuNCs in both investigated cell lines; however, AuNC-ZwBuEt did not induce cytotoxicity at 50 and 100  $\mu\text{g Au mL}^{-1}$ [23].

Furthermore, we previously showed that AuZwBuEt uptake in dendritic cells was both time- and concentration-dependent. It was observed that, initially, zwitterionic AuNCs enter the cell and are distributed throughout the cytoplasm, and then at a later stage, accumulate close to the nucleus. AuNCs were detected in different vesicles, including lysosome/terminal stage endocytic compartments but were not observed inside the nucleus or outside organelles (free within the cytoplasm)[38].

How the AuNCs trigger cell death upon cell entry still requires further investigation. Previous works have identified the role of lysosomal dysfunction that leads to lysosomal membrane permeability and the release of cathepsins into the cytosol, initiating cell apoptosis upon uptake of nanoparticles[53, 67]. However, in this work, we have identified impaired mitochondrial function (as determined by Cryo-SXT observations of mitochondria morphology, although no AuNC were found localised to mitochondria[49]) and cell vacuolisation due to AuNC exposure at 1 h post AuNC exposure, as well as a considerable accumulation of AuNC within lysosomes at 24 h and 4 days, post-exposure. Negatively charged Au nanoparticles that are internalized into cells and accumulate within lysosomes have been found to cause autophagosome accumulation resulting from the blockade of autophagy flux[68]. Additionally, the accumulation of NPs inside lysosomes results in lysosome destabilisation, swelling, and inhibition of autophagic flux[44]. The results of this study show that the fibroblasts triggered cell autophagy as a protective response. Autophagosomes ultimately fuse with lysosomes (autophagolysosomes) to degrade engulfed cytosolic contents. It is hypothesised that lysosomal dysfunction occurred, resulting in the observation of the AuNC-ZwBuEt accumulation in lysosomal vacuoles.

## Conclusion

This work investigated AuNC interactions with COS-7 fibroblasts by tuning cell-particle interactions using surface hydrophobicity/lipophilicity. The two AuNC-induced disparate responses in exposed COS-7 fibroblasts. In general, AuNC-MHA were not cytotoxic, even at the highest concentrations investigated, and were efficiently transported out of the cell following their uptake in endocytic vesicles. By contrast, AuNC-ZwBuEt were found to adversely impact the health of the fibroblasts. The slight decrease in hydrophobicity of AuNC-ZwBuEt led to efficient translocation of the particles through phospholipid membranes, allowing for their escape from endocytic vesicles. Single AuNC were also found localised to the nucleus after 24 h exposure, and cryo-SXT analysis showed severe cell stress response in the form of swollen mitochondria, nuclear membrane blebbing and the formation of large vacuoles. The ability of the AuNC to escape endosomes and translocate into the nucleus and other organelles may cause the observed cytotoxicity [69].

## References

- [1] L.V. Nair, R.V. Nair, S.J. Shenoy, A. Thekkuveetil, R.S. Jayasree, Blood brain barrier permeable gold nanocluster for targeted brain imaging and therapy: an in vitro and in vivo study, *Journal of Materials Chemistry B* 5(42) (2017) 8314-8321.
- [2] L. Shang, G.U. Nienhaus, Gold nanoclusters as novel optical probes for in vitro and in vivo fluorescence imaging, *Biophys Rev* 4(4) (2012) 313-322.
- [3] E. Porret, X. Le Guével, J.-L. Coll, Gold nanoclusters for biomedical applications: toward in vivo studies, *Journal of Materials Chemistry B* 8(11) (2020) 2216-2232.
- [4] Y. Zheng, J. Wu, H. Jiang, X. Wang, Gold nanoclusters for theranostic applications, *Coord. Chem. Rev.* 431 (2021) 213689.
- [5] L.-C. Cheng, X. Jiang, J. Wang, C. Chen, R.-S. Liu, Nano-bio effects: interaction of nanomaterials with cells, *Nanoscale* 5(9) (2013) 3547.
- [6] A. Cifuentes-Rius, V.G. Deepagan, J. Xie, N.H. Voelcker, Bright Future of Gold Nanoclusters in Theranostics, *ACS Applied Materials & Interfaces* 13(42) (2021) 49581-49588.
- [7] M.F. Matus, H. Häkkinen, Atomically Precise Gold Nanoclusters: Towards an Optimal Biocompatible System from a Theoretical-Experimental Strategy, *Small* 17(27) (2021) 2005499.
- [8] C.N. Loynachan, A.P. Soleimany, J.S. Dudani, Y. Lin, A. Najer, A. Bekdemir, Q. Chen, S.N. Bhatia, M.M. Stevens, Renal clearable catalytic gold nanoclusters for in vivo disease monitoring, *Nature Nanotechnology* 14(9) (2019) 883-890.
- [9] C. Colombé, X. Le Guével, A. Martin-Serrano, M. Henry, E. Porret, C. Comby-Zerbino, R. Antoine, I. Atallah, B. Busser, J.-L. Coll, C.A. Righini, L. Sancey, Gold nanoclusters as a

contrast agent for image-guided surgery of head and neck tumors, *Nanomed. Nanotechnol. Biol. Med.* 20 (2019) 102011.

[10] X. Le Guével, M. Henry, V. Motto-Ros, E. Longo, M.I. Montañez, F. Pelascini, O. de La Rochefoucauld, P. Zeitoun, J.-L. Coll, V. Josserand, L. Sancey, Elemental and optical imaging evaluation of zwitterionic gold nanoclusters in glioblastoma mouse models, *Nanoscale* 10(39) (2018) 18657-18664.

[11] Y. Chen, D.M. Montana, H. Wei, J.M. Cordero, M. Schneider, X. Le Guével, O. Chen, O.T. Bruns, M.G. Bawendi, Shortwave Infrared in Vivo Imaging with Gold Nanoclusters, *Nano Letters* 17(10) (2017) 6330-6334.

[12] Z. Yu, B. Musnier, K.D. Wegner, M. Henry, B. Chovelon, A. Desroches-Castan, A. Fertin, U. Resch-Genger, S. Bailly, J.-L. Coll, Y. Usson, V. Josserand, X. Le Guével, High-Resolution Shortwave Infrared Imaging of Vascular Disorders Using Gold Nanoclusters, *ACS Nano* 14(4) (2020) 4973-4981.

[13] S. Tang, C. Peng, J. Xu, B. Du, Q. Wang, R.D. Vinluan, M. Yu, M.J. Kim, J. Zheng, Tailoring Renal Clearance and Tumor Targeting of Ultrasmall Metal Nanoparticles with Particle Density, *Angewandte Chemie International Edition* 55(52) (2016) 16039-16043.

[14] D.F. Moyano, K. Saha, G. Prakash, B. Yan, H. Kong, M. Yazdani, V.M. Rotello, Fabrication of Corona-Free Nanoparticles with Tunable Hydrophobicity, *ACS Nano* 8(7) (2014) 6748-6755.

[15] Y. Genji Srinivasulu, Q. Yao, N. Goswami, J. Xie, Interfacial engineering of gold nanoclusters for biomedical applications, *Materials Horizons* 7(10) (2020) 2596-2618.

[16] B. Du, X. Jiang, A. Das, Q. Zhou, M. Yu, R. Jin, J. Zheng, Glomerular barrier behaves as an atomically precise bandpass filter in a sub-nanometre regime, *Nat Nanotechnol* 12(11) (2017) 1096-1102.

[17] K.L. Aillon, Y. Xie, N. El-Gendy, C.J. Berkland, M.L. Forrest, Effects of nanomaterial physicochemical properties on in vivo toxicity, *Adv. Drug Del. Rev.* 61(6) (2009) 457-466.

[18] H.S. Choi, W. Liu, P. Misra, E. Tanaka, J.P. Zimmer, B. Itty Ipe, M.G. Bawendi, J.V. Frangioni, Renal clearance of quantum dots, *Nat. Biotechnol.* 25(10) (2007) 1165-1170.

[19] C. Peng, Y. Huang, J. Zheng, Renal clearable nanocarriers: Overcoming the physiological barriers for precise drug delivery and clearance, *Journal of Controlled Release* 322 (2020) 64-80.

[20] X.-D. Zhang, Z. Luo, J. Chen, H. Wang, S.-S. Song, X. Shen, W. Long, Y.-M. Sun, S. Fan, K. Zheng, D.T. Leong, J. Xie, Storage of Gold Nanoclusters in Muscle Leads to their Biphasic in Vivo Clearance, *Small* 11(14) (2015) 1683-1690.

[21] Z. Liu, Z. Wu, Q. Yao, Y. Cao, O.J.H. Chai, J. Xie, Correlations between the fundamentals and applications of ultrasmall metal nanoclusters: Recent advances in catalysis and biomedical applications, *Nano Today* 36 (2021) 101053.

[22] B.D. Chithrani, A.A. Ghazani, W.C.W. Chan, Determining the Size and Shape Dependence of Gold Nanoparticle Uptake into Mammalian Cells, *Nano Letters* 6(4) (2006) 662-668.

[23] E. Porret, L. Sancey, A. Martín-Serrano, M.I. Montañez, R. Seeman, A. Yahia-Ammar, H. Okuno, F. Gomez, A. Ariza, N. Hildebrandt, J.-B. Fleury, J.-L. Coll, X. Le Guével, Hydrophobicity of Gold Nanoclusters Influences Their Interactions with Biological Barriers, *Chemistry of Materials* 29(17) (2017) 7497-7506.

[24] C.Y. Tay, Y. Yu, M.I. Setyawati, J. Xie, D.T. Leong, Presentation matters: Identity of gold nanocluster capping agent governs intracellular uptake and cell metabolism, *Nano Research* 7(6) (2014) 805-815.

[25] C. Carnovale, G. Bryant, R. Shukla, V. Bansal, Identifying Trends in Gold Nanoparticle Toxicity and Uptake: Size, Shape, Capping Ligand, and Biological Corona, *ACS Omega* 4(1) (2019) 242-256.

- [26] Y. Pan, A. Leifert, D. Ruau, S. Neuss, J. Bornemann, G. Schmid, W. Brandau, U. Simon, W. Jahnen-Dechent, Gold Nanoparticles of Diameter 1.4 nm Trigger Necrosis by Oxidative Stress and Mitochondrial Damage, *Small* 5(18) (2009) 2067-2076.
- [27] M. Turner, V.B. Golovko, O.P.H. Vaughan, P. Abdulkin, A. Berenguer-Murcia, M.S. Tikhov, B.F.G. Johnson, R.M. Lambert, Selective oxidation with dioxygen by gold nanoparticle catalysts derived from 55-atom clusters, *Nature* 454(7207) (2008) 981-983.
- [28] Y. Pan, S. Neuss, A. Leifert, M. Fischler, F. Wen, U. Simon, G. Schmid, W. Brandau, W. Jahnen-Dechent, Size-Dependent Cytotoxicity of Gold Nanoparticles, *Small* 3(11) (2007) 1941-1949.
- [29] M. Enea, E. Pereira, M. Peixoto de Almeida, A.M. Araújo, M.d.L. Bastos, H. Carmo, Gold Nanoparticles Induce Oxidative Stress and Apoptosis in Human Kidney Cells, *Nanomaterials* 10(5) (2020) 995.
- [30] R. Suresh Vs, Recent Advances on Renal Toxicity of Engineered Nanoparticles-A Review, *Journal of Toxicology and Risk Assessment* 7(1) (2021).
- [31] C. Peng, J. Xu, M. Yu, X. Ning, Y. Huang, B. Du, E. Hernandez, P. Kapur, J.T. Hsieh, J. Zheng, Tuning the In Vivo Transport of Anticancer Drugs Using Renal - Clearable Gold Nanoparticles, *Angew. Chem. Int. Ed.* 58(25) (2019) 8479-8483.
- [32] F. Strutz, G.A. Muller, Renal fibrosis and the origin of the renal fibroblast, *Nephrology Dialysis Transplantation* 21(12) (2006) 3368-3370.
- [33] D.P. Linklater, X. Le Guével, G. Bryant, V.A. Baulin, E. Pereiro, P.G.T. Perera, J.V. Wandiyanto, S. Juodkazis, E.P. Ivanova, Lethal Interactions of Atomically Precise Gold Nanoclusters and *Pseudomonas aeruginosa* and *Staphylococcus aureus* Bacterial Cells, *ACS Applied Materials & Interfaces* (2022).
- [34] D.P. Linklater, X. Le Guével, G. Bryant, V.A. Baulin, E. Pereiro, P.G.T. Perera, J.V. Wandiyanto, S. Juodkazis, E.P. Ivanova, Lethal Interactions of Atomically Precise Gold Nanoclusters and *Pseudomonas aeruginosa* and *Staphylococcus aureus* Bacterial Cells, *ACS Applied Materials & Interfaces* 14(28) (2022) 32634-32645.
- [35] X. Yuan, N. Goswami, W. Chen, Q. Yao, J. Xie, Insights into the effect of surface ligands on the optical properties of thiolated Au<sub>25</sub>nanoclusters, *Chem. Commun.* 52(30) (2016) 5234-5237.
- [36] M.R. Ivanov, A.J. Haes, Anionic Functionalized Gold Nanoparticle Continuous Full Filling Separations: Importance of Sample Concentration, *Anal. Chem.* 84(3) (2012) 1320-1326.
- [37] B. Musnier, K.D. Wegner, C. Comby-Zerbino, V. Trouillet, M. Jourdan, I. Häusler, R. Antoine, J.-L. Coll, U. Resch-Genger, X. Le Guével, High photoluminescence of shortwave infrared-emitting anisotropic surface charged gold nanoclusters, *Nanoscale* 11(25) (2019) 12092-12096.
- [38] T.D. Fernández, J.R. Pearson, M.P. Leal, M.J. Torres, M. Blanca, C. Mayorga, X. Le Guével, Intracellular accumulation and immunological properties of fluorescent gold nanoclusters in human dendritic cells, *Biomaterials* 43 (2015) 1-12.
- [39] Y. Yang, A. Han, R. Li, G. Fang, J. Liu, S. Wang, Synthesis of highly fluorescent gold nanoclusters and their use in sensitive analysis of metal ions, *The Analyst* 142(23) (2017) 4486-4493.
- [40] B. Dalzon, A. Torres, H. Diemer, S. Ravanel, V. Collin-Faure, K. Pernet-Gallay, P.-H. Jouneau, J. Bourguignon, S. Cianféroni, M. Carrière, C. Aude-Garcia, T. Rabilloud, How reversible are the effects of silver nanoparticles on macrophages? A proteomic-instructed view, *Environmental Science: Nano* 6(10) (2019) 3133-3157.
- [41] P. Tucci, G. Porta, M. Agostini, D. Dinsdale, I. Iavicoli, K. Cain, A. Finazzi-Agró, G. Melino, A. Willis, Metabolic effects of TiO<sub>2</sub> nanoparticles, a common component of

- sunscreens and cosmetics, on human keratinocytes, *Cell Death & Disease* 4(3) (2013) e549-e549.
- [42] W.E. Sinclair, H.-H. Chang, A. Dan, P.J.A. Kenis, C.J. Murphy, D.E. Leckband, Gold nanoparticles disrupt actin organization and pulmonary endothelial barriers, *Scientific Reports* 10(1) (2020).
- [43] T. Mironava, M. Hadjiargyrou, M. Simon, V. Jurukovski, M.H. Rafailovich, Gold nanoparticles cellular toxicity and recovery: Effect of size, concentration and exposure time, *Nanotoxicology* 4(1) (2010) 120-137.
- [44] M. Borkowska, M. Siek, D.V. Kolygina, Y.I. Sobolev, S. Lach, S. Kumar, Y.-K. Cho, K. Kandere-Grzybowska, B.A. Grzybowski, Targeted crystallization of mixed-charge nanoparticles in lysosomes induces selective death of cancer cells, *Nat Nanotechnol* 15(4) (2020) 331-341.
- [45] J. Groen, A. Palanca, A. Aires, J.J. Conesa, D. Maestro, S. Rehbein, M. Harkiolaki, A.V. Villar, A.L. Cortajarena, E. Pereiro, Correlative 3D cryo X-ray imaging reveals intracellular location and effect of designed antifibrotic protein–nanomaterial hybrids, *Chem Sci* 12(45) (2021) 15090-15103.
- [46] A. Nakashima, K. Higashisaka, T. Kusabiraki, A. Aoki, A. Ushijima, Y. Ono, S. Tsuda, T. Shima, O. Yoshino, K. Nagano, Y. Yoshioka, Y. Tsutsumi, S. Saito, Autophagy is a new protective mechanism against the cytotoxicity of platinum nanoparticles in human trophoblasts, *Scientific Reports* 9(1) (2019).
- [47] J. Xu, R. Camfield, S.M. Gorski, The interplay between exosomes and autophagy – partners in crime, *J. Cell Sci.* 131(15) (2018).
- [48] E.R. Gran, F. Bertorelle, H. Fakhouri, R. Antoine, M. Perić Bakulić, Ž. Sanader Maršić, V. Bonačić-Koutecký, M. Blain, J. Antel, D. Maysinger, Size and ligand effects of gold nanoclusters in alteration of organellar state and translocation of transcription factors in human primary astrocytes, *Nanoscale* 13(5) (2021) 3173-3183.
- [49] A. Gallud, K. Klöditz, J. Ytterberg, N. Östberg, S. Katayama, T. Skoog, V. Gogvadze, Y.-Z. Chen, D. Xue, S. Moya, J. Ruiz, D. Astruc, R. Zubarev, J. Kere, B. Fadeel, Cationic gold nanoparticles elicit mitochondrial dysfunction: a multi-omics study, *Scientific Reports* 9(1) (2019).
- [50] R. Rossignol, R. Gilkerson, R. Aggeler, K. Yamagata, S.J. Remington, R.A. Capaldi, Energy Substrate Modulates Mitochondrial Structure and Oxidative Capacity in Cancer Cells, *Cancer Res.* 64(3) (2004) 985-993.
- [51] T. Farmer, N. Naslavsky, S. Caplan, Tying trafficking to fusion and fission at the mighty mitochondria, *Traffic* 19(8) (2018) 569-577.
- [52] J. Cheng, Q. Zhang, S. Fan, A. Zhang, B. Liu, Y. Hong, J. Guo, D. Cui, J. Song, The vacuolization of macrophages induced by large amounts of inorganic nanoparticle uptake to enhance the immune response, *Nanoscale* 11(47) (2019) 22849-22859.
- [53] S.T. Stern, P.P. Adisheshaiah, R.M. Crist, Autophagy and lysosomal dysfunction as emerging mechanisms of nanomaterial toxicity, *Particle and Fibre Toxicology* 9(1) (2012) 20.
- [54] R. Andrade, L. Crisol, R. Prado, M.D. Boyano, J. Arluzea, J. Aréchaga, Plasma membrane and nuclear envelope integrity during the blebbing stage of apoptosis: a time - lapse study, *Biol. Cell* 102(1) (2010) 25-35.
- [55] Y. Guo, E. Terazzi, R. Seemann, J.B. Fleury, V.A. Baulin, Direct proof of spontaneous translocation of lipid-covered hydrophobic nanoparticles through a phospholipid bilayer, *Sci Adv* 2(11) (2016) e1600261-e1600261.
- [56] N. Gunduz, H. Ceylan, M.O. Guler, A.B. Tekinay, Intracellular Accumulation of Gold Nanoparticles Leads to Inhibition of Macropinocytosis to Reduce the Endoplasmic Reticulum Stress, *Scientific reports* 7 (2017) 40493-40493.



- [57] R. Gaspar, Pushed off target with proteins, *Nat Nanotechnol* 8(2) (2013) 79-80.
- [58] K.P. García, K. Zarschler, L. Barbaro, J.A. Barreto, W. O'Malley, L. Spiccia, H. Stephan, B. Graham, Zwitterionic-Coated "Stealth" Nanoparticles for Biomedical Applications: Recent Advances in Countering Biomolecular Corona Formation and Uptake by the Mononuclear Phagocyte System, *Small* 10(13) (2014) 2516-2529.
- [59] B. Musnier, K.D. Wegner, C. Comby-Zerbino, V. Trouillet, M. Jourdan, I. Hausler, R. Antoine, J.L. Coll, U. Resch-Genger, X. Le Guevel, High photoluminescence of shortwave infrared-emitting anisotropic surface charged gold nanoclusters, *Nanoscale* 11(25) (2019) 12092-12096.
- [60] E. Porret, L. Sancey, A. Martín-Serrano, M.I. Montañez, R. Seeman, A. Yahia-Ammar, H. Okuno, F. Gomez, A. Ariza, N. Hildebrandt, J.B. Fleury, J.L. Coll, X. Le Guével, Hydrophobicity of Gold Nanoclusters Influences Their Interactions with Biological Barriers, *Chemistry of Materials* 29(17) (2017) 7497-7506.
- [61] D.P. Linklater, X. Le Guével, G. Bryant, V.A. Baulin, E. Pereiro, P.G.T. Perera, J.V. Wandiyanto, S. Juodkazis, E.P. Ivanova, Lethal Interactions of Atomically Precise Gold Nanoclusters and *Pseudomonas aeruginosa* and *Staphylococcus aureus* Bacterial Cells, *ACS Applied Materials & Interfaces* 14(28) (2022) 32634-32645.
- [62] A.M. Smith, K.A. Johnston, S.E. Crawford, L.E. Marbella, J.E. Millstone, Ligand density quantification on colloidal inorganic nanoparticles, *Analyst* 142(1) (2017) 11-29.
- [63] A. Verma, O. Uzun, Y. Hu, Y. Hu, H.-S. Han, N. Watson, S. Chen, D.J. Irvine, F. Stellacci, Surface-structure-regulated cell-membrane penetration by monolayer-protected nanoparticles, *Nat. Mater.* 7(7) (2008) 588-595.
- [64] R.C. Van Lehn, P.U. Atukorale, R.P. Carney, Y.-S. Yang, F. Stellacci, D.J. Irvine, A. Alexander-Katz, Effect of Particle Diameter and Surface Composition on the Spontaneous Fusion of Monolayer-Protected Gold Nanoparticles with Lipid Bilayers, *Nano Letters* 13(9) (2013) 4060-4067.
- [65] E. Canepa, S. Salassi, F. Simonelli, R. Ferrando, R. Rolandi, C. Lambruschini, F. Canepa, S. Dante, A. Relini, G. Rossi, Non-disruptive uptake of anionic and cationic gold nanoparticles in neutral zwitterionic membranes, *Scientific Reports* 11(1) (2021).
- [66] E. Porret, L. Sancey, A. Martín-Serrano, M.I. Montañez, R. Seeman, A. Yahia-Ammar, H. Okuno, F. Gomez, A. Ariza, N. Hildebrandt, J.-B. Fleury, J.-L. Coll, X. Le Guével, Hydrophobicity of Gold Nanoclusters Influences Their Interactions with Biological Barriers, *Chem. Mater.* 29(17) (2017) 7497-7506.
- [67] F. Wang, A. Salvati, P. Boya, Lysosome-dependent cell death and deregulated autophagy induced by amine-modified polystyrene nanoparticles, *Open Biology* 8(4) (2018) 170271.
- [68] X. Ma, Y. Wu, S. Jin, Y. Tian, X. Zhang, Y. Zhao, L. Yu, X.-J. Liang, Gold Nanoparticles Induce Autophagosome Accumulation through Size-Dependent Nanoparticle Uptake and Lysosome Impairment, *ACS Nano* 5(11) (2011) 8629-8639.
- [69] M. Tsoi, H. Kuhn, W. Brandau, H. Esche, G. Schmid, Cellular Uptake and Toxicity of Au<sub>55</sub> Clusters, *Small* 1(8-9) (2005) 841-844.